AD-A036 142 CALIFORNIA UNIV LOS ANGELES SCHOOL OF ENGINEERING A--ETC F/G 11/2
FRACTURE STATISTICS OF BRITTLE MATERIALS WITH SURFACE CRACKS.(U)
JAN 77 S B BATDORF, H L HEINISCH, W J KNAPP N00014-76-C-0445

UNCLASSIFIED UCLA-ENG-7703 NL

1 OF 1
AD A036142

END
DATE FILMED
3-77

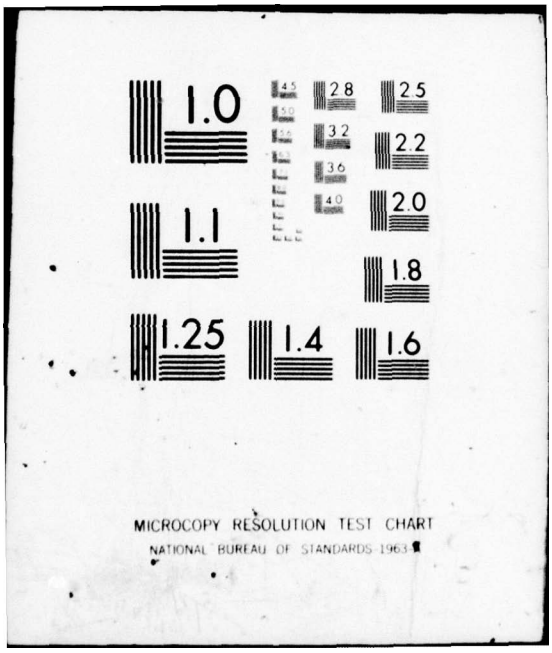
1.0
1.1
1.25
1.4
1.6
1.8
2.0
2.2
2.5
2.8
3.2
3.6
4.0
MICROCOPY RESOLUTION TEST CHART
NATIONAL BUREAU OF STANDARDS-1963-A

UCLA-ENG-7703
JANUARY 1977

FRACTURE STATISTICS OF BRITTLE MATERIALS WITH SURFACE CRACKS

S.B. BATDORF
H.L. HEINISCH, JR.

SECURITY CLASSIFICATION OF THIS PAGE *(When Data Entered)*

REPORT DOCUMENTATION PAGE

READ INSTRUCTIONS BEFORE COMPLETING FORM

1. REPORT NUMBER: UCLA-ENG-7703	2. GOVT ACCESSION NO.
3. RECIPIENT'S CATALOG NUMBER: rept.	
4. TITLE *(and Subtitle)*: FRACTURE STATISTICS OF BRITTLE MATERIALS WITH SURFACE CRACKS.	5. TYPE OF REPORT & PERIOD COVERED: Technical 1976-1977
	6. PERFORMING ORG. REPORT NUMBER: UCLA-ENG-7703
7. AUTHOR(s): S.B. Batdorf and H. L. Heinisch, Jr. W. J. Knapp	8. CONTRACT OR GRANT NUMBER(s): N00014-76-C-0445
9. PERFORMING ORGANIZATION NAME AND ADDRESS: School of Engineering and Applied Science, University of California, Los Angeles, California	10. PROGRAM ELEMENT, PROJECT, TASK AREA & WORK UNIT NUMBERS
11. CONTROLLING OFFICE NAME AND ADDRESS	12. REPORT DATE: January 1977 13. NUMBER OF PAGES: 29 p.
14. MONITORING AGENCY NAME & ADDRESS *(if different from Controlling Office)*: Department of Navy	15. SECURITY CLASS. *(of this report)*: Unclassified 15a. DECLASSIFICATION/DOWNGRADING SCHEDULE

16. DISTRIBUTION STATEMENT *(of this Report)*

Distribution is unlimited

17. DISTRIBUTION STATEMENT *(of the abstract entered in Block 20, if different from Report)*

18. SUPPLEMENTARY NOTES

19. KEY WORDS *(Continue on reverse side if necessary and identify by block number)*

material failure
brittle fracture
fracture statistics
statistical failure theory
ceramic fracture
fracture

20. ABSTRACT *(Continue on reverse side if necessary and identify by block number)*

Several different statistical fracture theories are developed for materials with cracks confined to the surface. All assume that crack planes are normal to the surface, but are otherwise randomly oriented. The simplest theory assumes that only the component of stress normal to the crack plane contributes to fracture. This theory is in fair agreement with biaxial fracture data on pyrex glass obtained by Oh. When the contribution of shear is included in the analysis, the crack

→ next page

DD FORM 1 JAN 73 1473 EDITION OF 1 NOV 65 IS OBSOLETE
S/N 0102-LF-014-6601

4042637

SECURITY CLASSIFICATION OF THIS PAGE *(When Data Entered)*

cont.

shape has to be considered. Several shapes are examined, and the corresponding fracture statistics are derived. The failure criterion employed is that fracture occurs when the maximum tensile stress on some part of the crack surface reaches the intrinsic strength of the material. The assumption of shear-sensitive cracks leads to improved agreement with experiment, but really good agreement appears to require the assumption that the cracks have a preferred orientation.

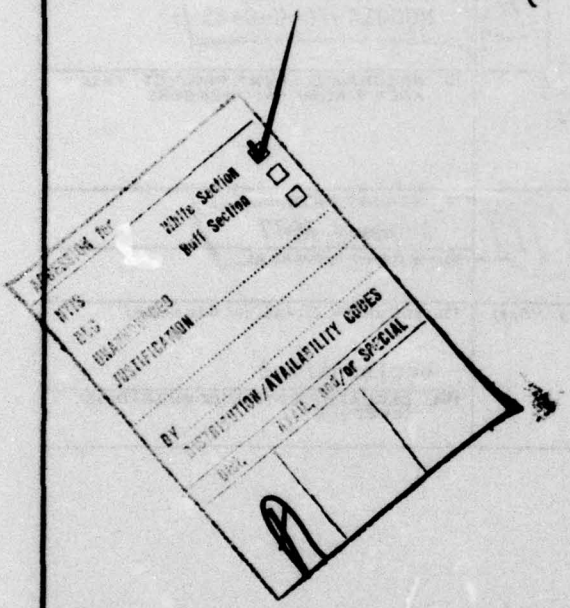

UCLA-ENG-7703
JANUARY 1977

FRACTURE STATISTICS OF BRITTLE MATERIALS

WITH SURFACE CRACKS

S.B. Batdorf and H.L. Heinisch, Jr.

Sponsored by the
Department of the Navy
Office of Naval Research
under Contract No. N00014-76-C-0445

Co-Sponsored by
Air Force Office of Scientific Research

School of Engineering and Applied Science
University of California
Los Angeles, California

ABSTRACT

Several different statistical fracture theories are developed for materials with cracks confined to the surface. All assume that crack planes are normal to the surface, but are otherwise randomly oriented. The simplest theory assumes that only the component of stress normal to the crack plane contributes to fracture. This theory is in fair agreement with biaxial fracture data on pyrex glass obtained by Oh. When the contribution of shear is included in the analysis, the crack shape has to be considered. Several shapes are examined, and the corresponding fracture statistics are derived. The failure criterion employed is that fracture occurs when the maximum tensile stress on some part of the crack surface reaches the intrinsic strength of the material. The assumption of shear-sensitive cracks leads to improved agreement with experiment, but really good agreement appears to require the assumption that the cracks have a preferred orientation.

TABLE OF CONTENTS

		Page
Figures		vii
I.	Introduction	1
II.	Theory: Shear on Crack Plane Neglected	2
III.	Oh's Theory	7
IV.	Present Theory	9
V.	Concluding Discussion	20
References		21

LIST OF FIGURES

Page

Fig. 1 Probability of failure for pyrex tubes under biaxial tensile stress states 1:1, 1:0.5, and 1:0 assuming only normal components of stress on the cracks contribute to failure. The curves for 1:0.5, and 1:0 are generated from the curve for 1:1, which is fitted to the experimental results of Oh (1970). Data points for the three stress states are plotted. 6

Fig. 2 Failure probability curves fitted to 1:1 data of Oh (1970). Curve (O) is determined from parameters reported by Oh for the three-parameter Weibull function $P_f = 1 - \exp\{-((\sigma - \sigma_u)/\sigma_0)^m\}$. Curve (A) is a Weibull function, and (B) is a piecewise function consisting of two Weibull curves joined by a straight line such that P_f and its slope remain continuous. The values of the parameters are as follows:

O:	$\sigma_u = 1.50$	$\sigma_0 = 3.32$	$m = 2.20$	
A:	$\sigma_u = 0.25$	$\sigma_0 = 4.64$	$m = 3.60$	
B:	$\sigma_u = 0.50$	$\sigma_0 = 4.45$	$m = 2.73$	$\sigma_u \leq \sigma < 3.5$
	$P_f = 0.221(\sigma - 0.5) - 0.373$			$3.5 \leq \sigma < 6.0$
	$\sigma_u = 0.50$	$\sigma_0 = 4.69$	$m = 4.02$	$6.0 \leq \sigma < \infty$

8

Fig. 3 Probability of failure for uniaxial tension by Oh's method. The curves labeled A(1:0), B(1:0) and O(1:0) are Weibull functions whose parameters are determined graphically from computed values of $P_f << 0.01$ starting from the A(1:1), B(1:1), and O(1:1) fits to the equibiaxial data, respectively. The unlabeled curve was plotted using the Weibull parameters for 1:0 reported by Oh. 10

Fig. 4 Surface crack models: (a) Griffith through-crack, (b) Griffith notch, (c) half ellipsoid. P_1, P_2, P_3 indicate the locations of the maximum stress in each model. P_3 lies in the $X_1 - X_3$ plane, but not on the X_1 axis when shear is present. Its exact position depends on the stress state 11

Fig. 5 Failure probability curves for uniaxial tension (1:0) determined from the B(1:1) fit to the equibiaxial data assuming three different crack models: the shear insensitive (SI), the Griffith notch (GN), and the half-ellipsoid (HE). The points are the 1:0 data of Oh (1970). 15

LIST OF FIGURES (Cont'd)

Page

Fig. 6. Failure probability curves for uniaxial tension calculated using the B(1:1) fit to the equibiaxial data for Griffith notch cracks assuming a simple anisotropy of crack orientation in which the cracks are uniformly distributed over only a certain fraction R of the possible angular orientations. Curves for R = .6 and R = .75 are shown in comparison to the data points. 18

Fig. 7 Failure probability curves for stress state 1:0.5 for isotropically and anisotropically (R = .6) distributed cracks calculated using the B(1:1) fit to the equibiaxial data. The points are the 1:0.5 data of Oh (1970). 19

I. INTRODUCTION

There are many cases in which structures must be fabricated using brittle materials. The strongest and most refractory materials tend to be brittle. Also, materials transparent to microwave, infrared, or visible radiation are generally brittle. Brittle structures characteristically exhibit a large variation in fracture stress which must be taken into account in design.

The most widely used statistical theory of fracture is due to Weibull (1939). He attributed the variation in fracture stress of nominally identical specimens to the presence of unidentified, invisible flaws. The flaws were assumed to have a distribution in strength, and the specimen or structure was assumed to fail when the strength of the weakest flaw or link was exceeded.

Batdorf and Crose (1974) revised weakest link theory by assuming the flaws to be cracks, and therefore to have strengths which depend on the orientation of the cracks with respect to the applied stresses. All orientations were considered equally likely, i.e., the material was assumed to be macroscopically isotropic. It was further assumed that only the component of stress normal to the crack plane contributed to fracture. The latter assumption was a convenient approximation which permitted development of a general theory without having to specify crack shapes. The shear parallel to the crack plane also contributes to the fracture, but by an amount that depends on the crack shape, which is something one usually does not know. In some cases, however, we may be able to derive information about crack shapes by examining the fracture statistics for a number of different stress states.

Only volume distributed cracks were treated by Batdorf and Crose (1974). In the case of some materials, e.g., glass, it is generally accepted that all cracks are located at the surface, and also that the crack planes are normal to the glass surface (McClintock and Argon, 1966). For such materials

the crack orientation is given by a single parameter rather than two, as in the case of volume distributed cracks.

In the present paper the theory of Batdorf and Crose is modified for surface distributed cracks and is applied to fracture data for glass obtained by Oh (Oh, 1970; Oh et al., 1973). The agreement with experiment leaves something to be desired. It is evident that including the effects of shear on the crack plane would decrease the discrepancy.

A more refined theory including the influence of shear and based on the assumption that the cracks are Griffith cracks and that failure occurs when the local tensile stress on the crack surface exceeds the intrinsic strength of the material was developed by Oh (1970). Some improvement in agreement with test data resulted. The present authors believe that the crack model employed by Oh is not appropriate for surface cracks. Alternative models are therefore proposed, but the improvement is marginal. Good agreement with experiment is obtained by assuming that in addition to being shear-sensitive, the cracks have a preferred orientation.

II. THEORY: SHEAR ON CRACK PLANE NEGLECTED

Consider first a single crack of arbitrary orientation. Since it is assumed to be small and located at the surface, it is subjected at most to plane stress. In the principal axis system, the tensile component of stress normal to the crack line and in the plane of the surface is

$$\sigma_n = \sigma_x \cos^2\theta + \sigma_y \sin^2\theta \tag{1}$$

where θ is the angle between the x-axis and the crack normal. In accordance with the preceding assumptions, the material will rupture when $\sigma_n > \sigma_{cr}$ where σ_{cr} is the macroscopic normal stress required to rupture the crack. If the crack is randomly oriented, the probability of failure is given by

$$P_f = \frac{\omega}{\pi} \tag{2}$$

where ω is the radian measure of the angular range in the positive σ_x half-plane within which $\sigma_n > \sigma_{cr}$.

In a real material, there will be a number of cracks of varying orientation and critical stress. If we assume that the cracks are uniformly distributed over the surface, the material can be characterized by a density function $N\left(\sum, \sigma_{cr}\right)$ where $\sum$ is the applied stress state. This function represents the number of cracks per unit area having a critical stress less than or equal to σ_{cr}. The number of cracks per unit area having critical stresses between σ_{cr} and $\sigma_{cr} + d\sigma_{cr}$ is, then,

$$dN = \frac{dN}{d\sigma_{cr}} d\sigma_{cr} \tag{3}$$

The probability that failure will occur in a uniformly stressed surface of area A due to a crack having a critical stress in the range σ_{cr} to $\sigma_{cr} + d\sigma_{cr}$ is the product of the probability that a crack is present and the probability that the crack, if present, will fail; i.e.,

$$P_f\left(\sum, d\sigma_{cr}\right) = \left(A \frac{dN}{d\sigma_{cr}} d\sigma_{cr}\right)\left(\frac{\omega}{\pi}\right) \tag{4}$$

The probability that such cracks will survive is

$$P_s\left(\sum, d\sigma_{cr}\right) = 1 - P_f = 1 - A \frac{\omega}{\pi} \frac{dN}{d\sigma_{cr}} d\sigma_{cr}$$

$$\cong \exp\left[- A \frac{\omega}{\pi} \frac{dN}{d\sigma_{cr}} d\sigma_{cr}\right] \tag{5}$$

The probability that cracks in every stress range $d\sigma_{cr}$ will survive is the product of the probabilities of survival of cracks in the individual ranges, i.e.,

$$P_s = \exp\left[-A \int \frac{\omega}{\pi} \frac{dN}{d\sigma_{cr}} d\sigma_{cr}\right] = 1 - P_f \tag{6}$$

The fracture probability for a surface of area A subjected to stress state Σ can be evaluated with the use of Eq. (6) when ω and N are known. For any stress state Σ, we can determine ω by using Eq. (1), while N must be obtained by experiment.

In the uniaxial case, Eq. (1) reduces to

$$\sigma_n = \sigma_x \cos^2\theta$$

Thus for this case, $\pm\theta_{cr}$, the angle within which $\sigma_n > \sigma_{cr}$, is given by

$$\sigma_{cr} = \sigma_x \cos^2\theta_{cr}$$

or

$$\theta_{cr} = \cos^{-1}\sqrt{\frac{\sigma_{cr}}{\sigma_x}} \tag{7}$$

Since $\omega = 2\theta_{cr}$,

$$\frac{\omega}{\pi} = \frac{2}{\pi}\cos^{-1}\sqrt{\frac{\sigma_{cr}}{\sigma_x}} \tag{8}$$

In the equibiaxial case,

$$\sigma_x = \sigma_y = \sigma \tag{9}$$

as a result of which, $\sigma_n = \sigma$ and

$$\frac{\omega}{\pi} = 1 \text{ for } \sigma_{cr} < \sigma \tag{10a}$$

$$= 0 \text{ for } \sigma_{cr} > \sigma \tag{10b}$$

As a result of (10a, b), in the equibiaxial tension case Eq. (6) takes the simple form

$$P_f(\sigma) = 1 - \exp[-AN(\sigma)] \tag{11}$$

From a comparison of Eqs. (6) and (8) with (11), it becomes clear that it is computationally advantageous to determine N from the fracture statistics for equal biaxial tension. From (11), we find AN is given by

$$AN = \ell n(1 - P_f)^{-1} \tag{12}$$

thereby avoiding the necessity encountered in the theory of volume-distributed cracks of solving simultaneous linear algebraic equations or an integral equation to obtain N. Actually, in the volume distribution case, a simplification like Eq. (12) occurs for equitriaxial tension, but this state of stress cannot be realized in practice.

Under general biaxial stress states, Eq. (1) can be rewritten as

$$\sigma_n = \sigma_x(\cos^2\theta + K \sin^2\theta) = \sigma_x[\cos^2\theta(1 - K) + K] \tag{13}$$

where

$$K = \frac{\sigma_y}{\sigma_x} \tag{14}$$

Thus,

$$\theta_{cr} = \cos^{-1}\sqrt{\frac{\left(\sigma_{cr}/\sigma_x\right) - K}{1 - K}} \tag{15}$$

$$\frac{\omega}{\pi} = \frac{2}{\pi}\cos^{-1}\sqrt{\frac{\left(\sigma_{cr}/\sigma_x\right) - K}{1 - K}} \tag{16}$$

Using Eqs. (6), (12), and (16) we can obtain the probability of failure of a surface of area A subject to biaxial tension.

The results of the theory just outlined are compared with the experimental results of Oh in Figure 1. It is evident that although the general trend of the theoretical results are in accord with the data, the theoretical curves for stress ratios 1:1, 1:0.5, and 1:0 are too far apart. Taking account of the contribution of shear on a crack to the failure process would increase the probability of failure for stress ratios 1:0.5 and 1:0, and therefore bring the curves closer together. We therefore turn to theories in which shear effects are taken into account.

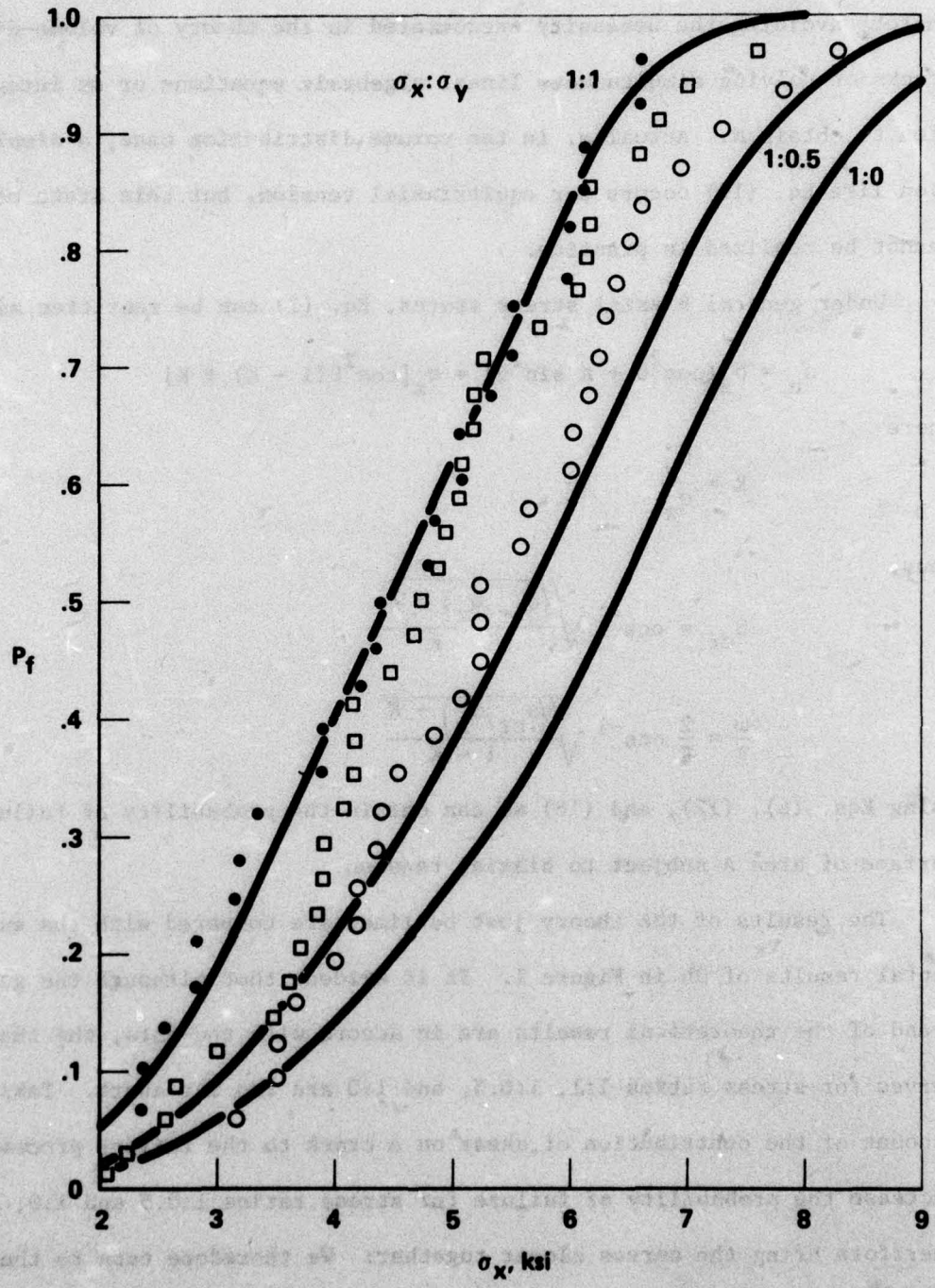

Figure 1. Probability of Failure for Pyrex Tubes Under Biaxial Tensile Stress States 1:1, 1:0.5, and 1:0 Assuming Only Normal Components of Stress on the Cracks Contribute to Failure. The curves for 1:0.5 and 1:0 are generated from the curve for 1:1, which is fitted to the experimental results of Oh (1970). Data points for the three stress states are plotted.

III. OH'S THEORY

It was shown by Oh (1970) that when a Griffith crack is subjected to principal stresses σ_x and σ_y, the maximum tensile stress at any point on the surface of a crack is (in our notation)

$$\sigma_{max} = \frac{1}{\xi}\left(T + \sqrt{T^2 + S^2}\right) \tag{17a}$$

where the tensile and shear forces on the crack are given by

$$T = \sigma_x\left(\frac{1 + K}{2} + \frac{1 - K}{2}\cos 2\theta\right) \tag{17b}$$

$$S = \sigma_x\left(\frac{1 - K}{2}\sin 2\theta\right) \tag{17c}$$

In these equations $K \equiv \sigma_y/\sigma_x < 1$, ξ is the ratio of the minor to the major axis of the ellipse, while θ is the complement of the angle between the larger principal stress and the crack plane. All values of θ were assumed equally likely, and the distribution of cracks with respect to ξ was chosen to fit a three-parameter Weibull representation of the data for the stress ratio 1:1.

To obtain the failure probabilities for stress ratios 1:0.5 and 1:0 it was arbitrarily assumed that these would also be three-parameter Weibull distributions. The corresponding parameters were found by applying the graphical approach for Weibull parameter estimation to synthetic data computed for $P_f << 0.01$. Such a procedure would be theoretically justified if failure always occurred for $\sigma_x - \sigma_u << \sigma_u$, a condition not applying to Oh's data. In spite of this, when the procedure is applied using Oh's Weibull parameters for equibiaxial tension, good agreement is obtained with uniaxial test data. However, two other fits to the equibiaxial data were devised by the present authors (Figure 2). One, labeled A, is an alternative Weibull function. The other, labeled B and identified in Figure 2, is a closer fit to the data, but also more complicated than any Weibull function. Although the three fits to

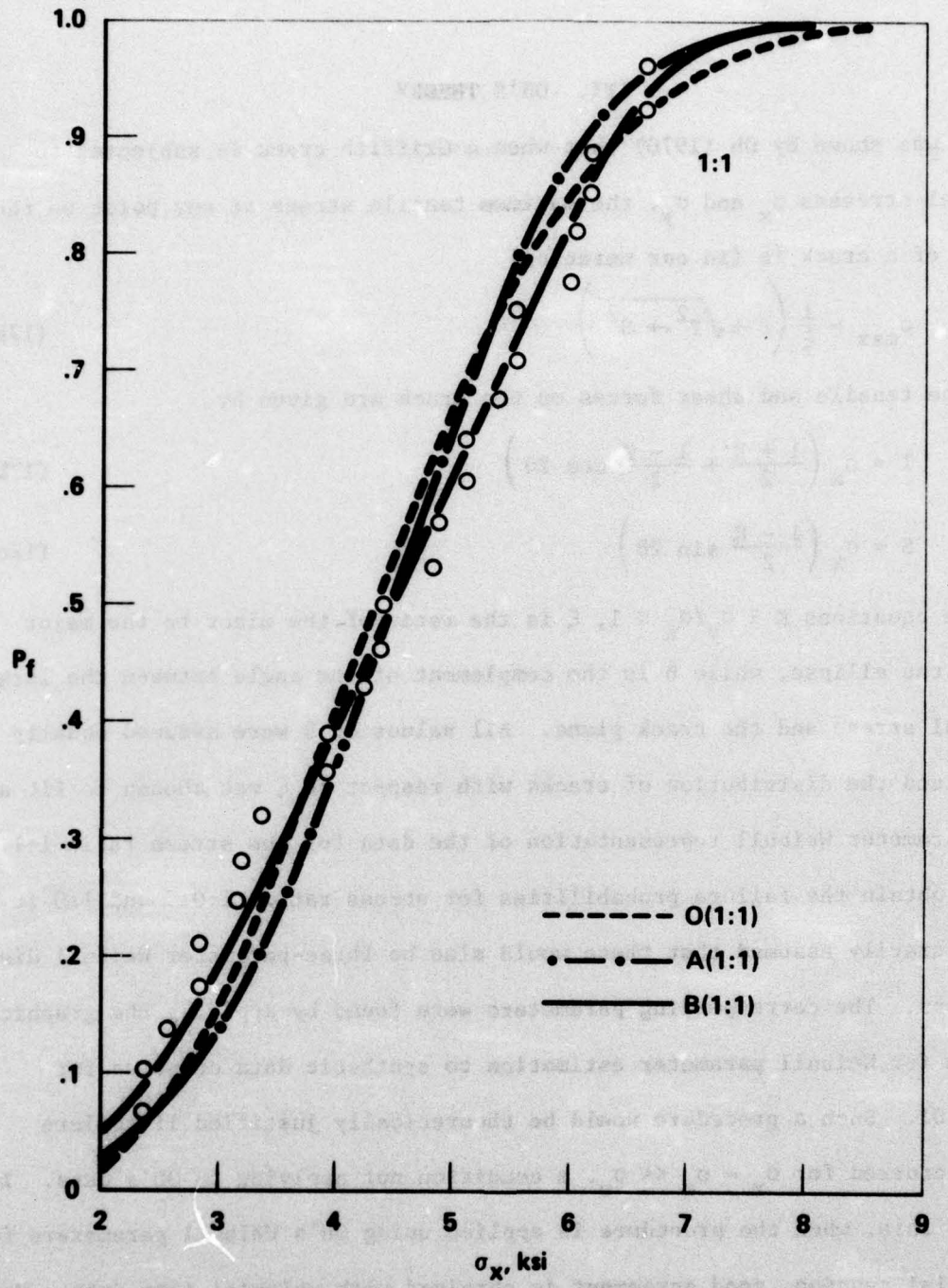

Figure 2. **Failure Probability Curves Fitted to 1:1 Data of Oh (1970). Curve (0) is determined from parameters reported by Oh for the three-parameter Weibull function $P_f = 1 - \exp\{-((\sigma-\sigma_u)/\sigma_0)^m\}$. Curve (A) is a Weibull function, and (B) is a piecewise function consisting of two Weibull curves joined by a straight line such that P_f and its slope remain continuous. The values of the parameters are as follows:**

0:	$\sigma_u = 1.50$	$\sigma_0 = 3.32$	$m = 2.20$	
A:	$\sigma_u = 0.25$	$\sigma_0 = 4.64$	$m = 3.60$	
B:	$\sigma_u = 0.50$	$\sigma_0 = 4.45$	$m = 2.73$	$\sigma_u \leq \sigma < 3.5$
	$P_f = 0.221\,(\sigma-0.5) - 0.373$			$3.5 \leq \sigma < 6.0$
	$\sigma_u = 0.50$	$\sigma_0 = 4.69$	$m = 4.02$	$6.0 \leq \sigma < \infty$

the 1:1 data are quite close, the Oh procedure leads to very significant differences in the predicted uniaxial failure curves for the three cases, as shown in Figure 3. This suggests that the good agreement found using Oh's function may be fortuitous.

Oh's analysis is based on the tacit assumption that the Griffith crack is a through-crack (Figure 4a). This is not considered by the present authors to be an appropriate model for the surface crack. Section IV is concerned with two other types of cracks illustrated in Figures 4b and 4c. The first, which we shall call a Griffith notch, is a half-elliptic cylinder with the principal axis of the cylinder at the surface of the specimen. The second is a half-ellipsoid in which $a >> b >> c$.

IV. PRESENT THEORY

A fracture criterion under combined stress can be formulated on any of several different bases. These include use of an energy criterion, use of critical stress concentration factors, and use of maximum tensile stress occurring at a point on a surface of the crack. The simplest one of these to apply is the last.

Mirandy and Paul (1975; also Paul and Mirandy, 1975) have recently worked out the stress state at any point on the surface of an ellipsoidal cavity having axes a, b, and c, such that $c << b \leq a$ for arbitrary applied stresses. For present purposes the principal findings are: (1) If the applied stress is simple tension T normal to the plane of the crack (i.e., parallel to the polar or c-axis of the crack), the maximum stress occurs at the intersection of the cavity and the a-b or equatorial plane. The local stress is the same at all points in the equatorial plane and is given by

$$\sigma = \frac{b}{c} \frac{2T}{E} \tag{18}$$

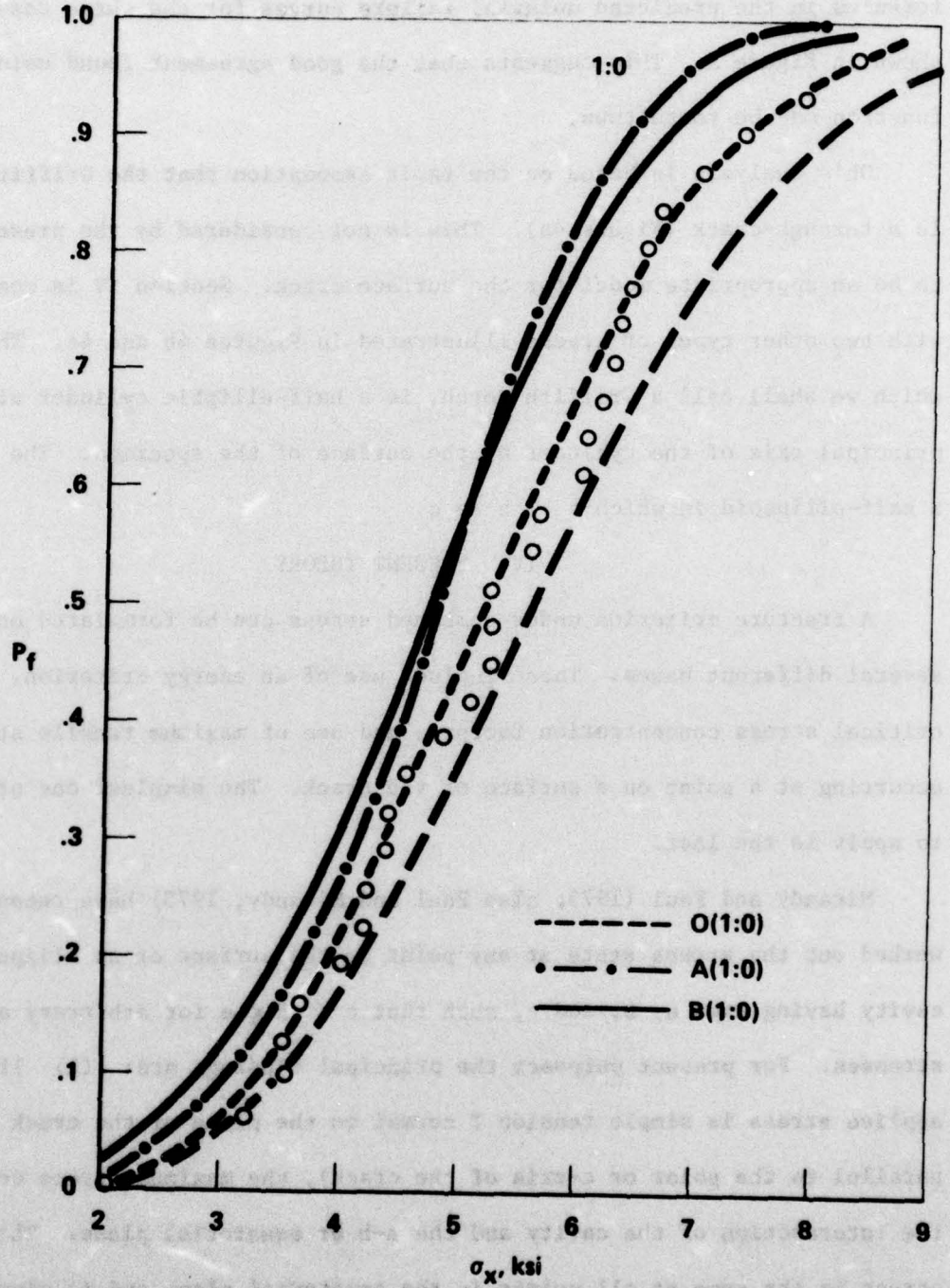

Figure 3. Probability of Failure for Uniaxial Tension by Oh's Method. The curves labeled A(1:0), B(1:0) and 0(1:0) are Weibull functions whose parameters are determined graphically from computed values of $P_f \ll 0.01$ starting from the A(1:1), B(1:1), and 0(1:1) fits to the equibiaxial data, respectively. The unlabeled curve was plotted using the Weibull parameters for 1:0 reported by Oh.

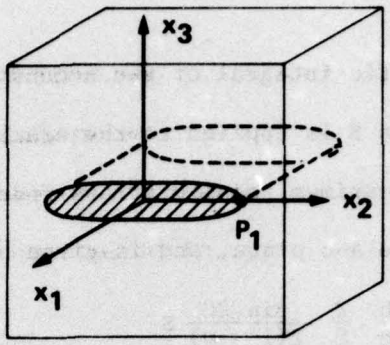

(a)

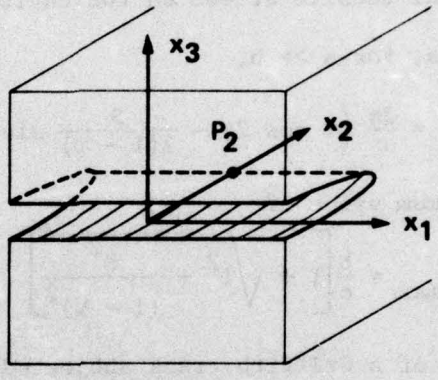

(b)

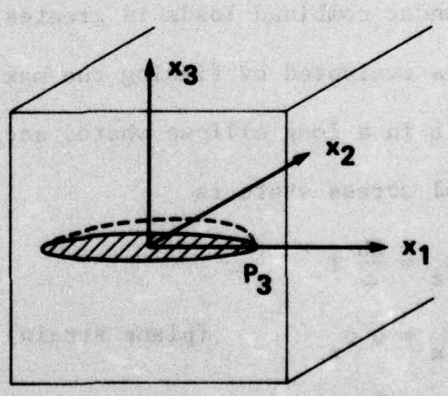

(c)

Figure 4. **Surface Crack Models: (a) Griffith Through-Crack, (b) Griffith Notch, (c) Half Ellipsoid. P_1, P_2, P_3 indicate the locations of the maximum stress in each model. P_3 lies in the X_1-X_3 plane, but not on the X_1 axis when shear is present. Its exact position depends on the stress state.**

where E is an elliptic integral of the second kind. For $b/a \ll 1$, $E = 1$.

(2) If shear stress S is applied to the crack plane in a direction parallel to the a-axis, the maximum tensile stress induced on the surface of the cavity occurs in the a-c plane, and is given by

$$\sigma = \frac{b}{c} \frac{2}{E} \frac{\sin 2\beta}{2(1 - \nu)} S \tag{19}$$

where β is the local latitude. (3) When both S and T as described above are present, the local tensile stress on the cavity surface is largest in the a-c plane and becomes, for $a \gg b$,

$$\sigma = \frac{2b}{c} \left(T \cos 2\beta - \frac{S}{2(1 - \nu)} \sin 2\beta \right) \tag{20}$$

which has a maximum value of

$$\sigma_{max} = \frac{b}{c} \left[T + \sqrt{T^2 + \frac{S^2}{(1 - \nu)^2}} \right] \tag{21}$$

(4) In the case of a Griffith crack subjected to tension normal to the crack plane and shear on the crack plane applied parallel to the cylinder axis, the tensile stress under combined loads is greatest along the line of maximum curvature. It is evaluated by finding the maximum principal stress at the end of the b-axis in a long ellipse where, according to Mirandy and Paul (1975), the local stress state is

$$\sigma_z = \frac{2b}{c} T \tag{22a}$$

$$\sigma_x = \nu \sigma_z \qquad \text{(plane strain)} \tag{22b}$$

$$\tau = \frac{b}{c} S \tag{22c}$$

Using Mohr's circle, this is readily shown to be

$$\sigma_{max} = \frac{b}{c} \left[T(1 + \nu) + \sqrt{T^2(1 - \nu)^2 + S^2} \right] \tag{23}$$

The above results are for ellipsoids in an isotropic elastic body located far from any free surfaces. In the case of surface cracks such as those shown in Figure 4, the presence of the free surface will modify to some degree the stresses on the surface of the half-ellipsoid and Griffith notch. An estimate of the amount of this modification can be made for the Griffith notch as follows: We note that as $a \to \infty$ the ellipsoid approaches an elliptic cylinder, so that (23) should be valid for the cylinder. In the case of the half cylinder (Griffith notch) of Figure 4b, it has been shown (Paris and Sih, 1965) that the free surface causes the stress concentration factor for tension to be increased by a factor of 1.12, while that for shear is unchanged. Thus, we modify (23) to read

$$\sigma_{max} = 1.12 \frac{b}{c} \left[T(1 + \nu) + \sqrt{T^2 (1 - \nu)^2 + \left(\frac{S}{1.12}\right)^2} \right] \tag{24}$$

This equation differs appreciably in appearance from that applying to the through-crack (17a). Among other things, it depends on Poisson's ratio. However, for the range of values appropriate to glass, $\nu = 0.2$ to 0.3, the relative contribution of the applied tensile and shear stresses to the maximum tensile stress on the surface of the cavity is almost the same.

The present method of determining failure probability curves for various stress states is to solve the integral in (6) numerically over the entire range of applied stress. The data for equibiaxial tension are used to determine $dN/d\sigma_{cr}$ via (12). While it is not necessary to assume a Weibull form for $P_f(\sigma)$, several Weibull fits to the data were investigated. The best fit, however, was a piecewise function defined over three regions of the applied stress range (Figure 2) and used exclusively in the computations of the present theory.

The fraction ω/π is a function of the applied stress state and σ_{cr} and is determined in the following manner. The maximum tensile stress on the surface of the crack (equations 17, 21 or 24) can be written as

$$\sigma_{max} = \frac{2}{\xi} \sigma_x \, g(\theta,K) \tag{25}$$

where $g(\theta,K)$ is the function of crack orientation θ and stress state K appropriate to the crack model and σ_x is the applied stress. The failure criterion is $\xi\sigma_{max} \geq 2\sigma_{cr}$ or $\sigma_x \, g(\theta,K) \geq \sigma_{cr}$. The fraction ω/π is the portion of the range $0 \leq \theta \leq \pi/2$ for which $g(\theta,K) \geq \sigma_{cr}/\sigma_x$, and in general can be determined from the roots of the nonlinear equation $g(\theta,K) = \sigma_{cr}/\sigma_x$ at each value of σ_{cr}/σ_x.

Figure 5 compares the failure probability curves for stress ratio 1:0 deduced from the experimental data for stress ratio 1:1 using (13), (21) and (24). The results using (21) are somewhat closer to the experimental data, but not much. A correction of unknown magnitude is needed to account for the presence of the free surface. Moreover, it is doubtful whether a fracture criterion should be based on a maximum stress occurring at the end of the major axis. If the material strength is exceeded there, the crack should lengthen along the surface but not penetrate in from the surface in the manner required to partition the specimen. Accordingly, we conclude that (24) is the more appropriate fracture criterion.

Use of the critical stress concentration factor for the fracture criterion leads to the same conclusion. The critical stress concentration factors for a notch subjected to tension and out-of-plane shear are (Paris and Sih, 1965).

$$K_I = 1.12 \, T\sqrt{\pi b} \tag{26}$$

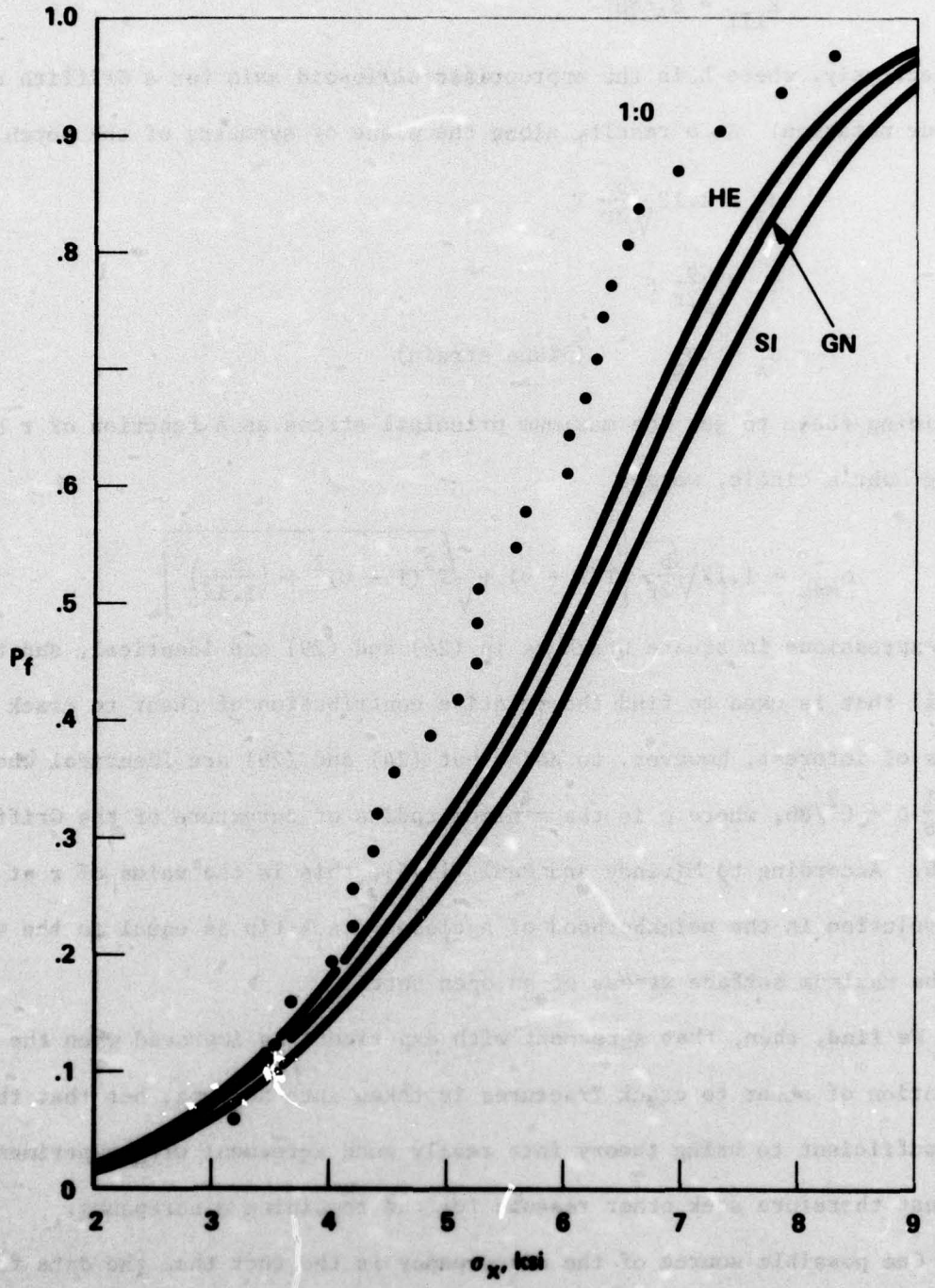

Figure 5. Failure Probability Curves for Uniaxial Tension (1:0) Determined from the B(1:1) Fit to the Equibiaxial Data Assuming Three Different Crack Models: the Shear Insensitive (SI), the Griffith Notch (GN), and the Half-Ellipsoid (HE). The points are the 1:0 data of Oh (1970).

and

$$K_{III} = S\sqrt{\pi b} \tag{27}$$

respectively, where b is the appropriate ellipsoid axis for a Griffith notch in our notation. As a result, along the plane of symmetry of the notch

$$\sigma_z = 1.12\sqrt{\frac{b}{2r}}\, T \tag{28a}$$

$$\tau = \sqrt{\frac{b}{2r}}\, S \tag{28b}$$

$$\sigma_x = \nu\sigma_z \qquad \text{(plane strain)} \tag{28c}$$

Combining these to get the maximum principal stress as a function of r by using Mohr's circle, we get

$$\sigma_{max} = 1.12\sqrt{\frac{b}{2r}}\left[T(1+\nu) + \sqrt{T^2(1-\nu)^2 + \left(\frac{S}{1.12}\right)^2}\right] \tag{29}$$

The expressions in square brackets in (24) and (29) are identical, and this is all that is used to find the relative contribution of shear to crack failure. It is of interest, however, to note that (24) and (29) are identical when $r = \frac{1}{8}\rho = C^2/8b$, where ρ is the minimum radius of curvature of the Griffith notch. According to Mirandy and Paul (1975), this is the value of r at which the solution in the neighborhood of a closed crack tip is equal to the value of the maximum surface stress of an open notch.

We find, then, that agreement with experiment is improved when the contribution of shear to crack fractures is taken into account, but that this is not sufficient to bring theory into really good agreement with experiment. We must therefore seek other reasons for the remaining discrepancy.

One possible source of the discrepancy is the fact that the data for failures at a stress ratio 1:1 cover a somewhat lower stress range than failures at stress ratio 1:0. Thus, an analytical expression for $AN(\sigma_{cr})$ obtained from 1:1 data should not be extrapolated to higher values of σ_{cr}.

However, the 1:1 failure stress range covers most of the 1:0 failure stress range so the agreement between theory and experiment in this large overlap region should be good, but it is not.

Another possible source for the discrepancy is the assumption in the theory that crack planes are always normal to the free surface of the material. This explanation also fails. It has been shown (by methods to be reported elsewhere) that the 1:0 failure curve deduced from 1:1 data is the same using the surface crack theory described here as it is using the volume distributed crack theory of Batdorf and Crose, employing a normal stress failure criterion in both cases.

The final possible explanation to be discussed here is that the assumption of uniform distribution of crack orientation is not valid for the pyrex tubes tested. There is no a priori method of predicting what form an anisotropic distribution should take. A crude but useful check on the hypothesis of anisotropy is to investigate the consequences of assuming that cracks are uniformly distributed through a given range of angles and are absent outside this range. For instance, one might assume that all crack planes are within ψ radians of the axis of the pyrex tubes, thus occupying a fraction $R = 2\psi/\pi$ of the total available angular orientation. Figures 6 and 7 show the results of assuming shear-sensitive Griffith notch cracks for $R = 0.6$ and $R = 0.75$. It is evident that the anisotropy assumption greatly improves agreement between theory and experiment. Unfortunately, the tubes were tested in simple tension in only one (the circumferential) direction, so that a direct test of the anisotropy hypothesis is lacking.

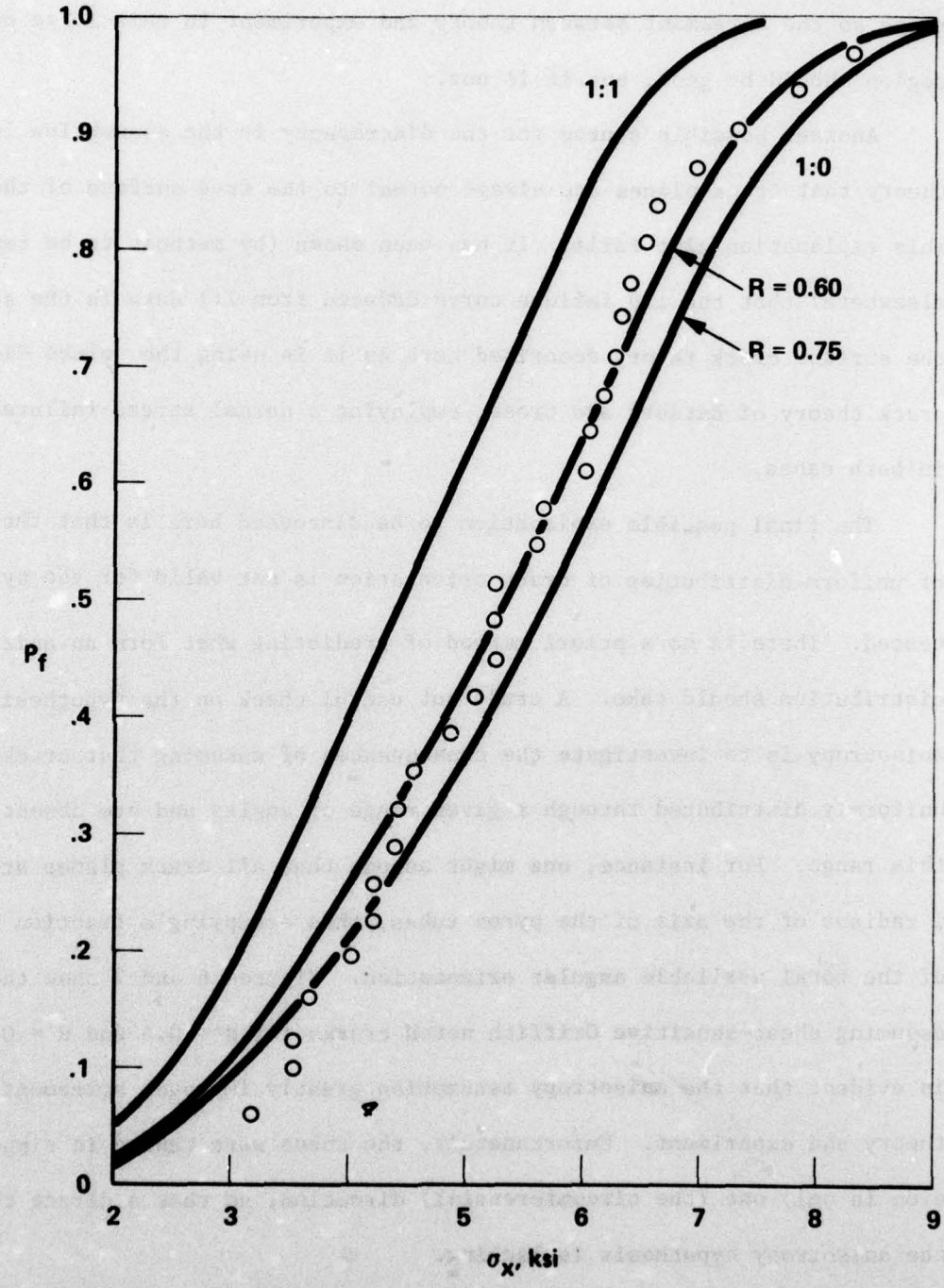

Figure 6. Failure Probability Curves for Uniaxial Tension Calculated Using the B(1:1) Fit to the Equibiaxial Data for Griffith Notch Cracks Assuming a Simple Anisotropy of Crack Orientation in Which the Cracks are Uniformly Distributed Over Only a Certain Fraction R of the Possible Angular Orientations. Curves for R = .6 and R = .75 are shown in comparison to the data points.

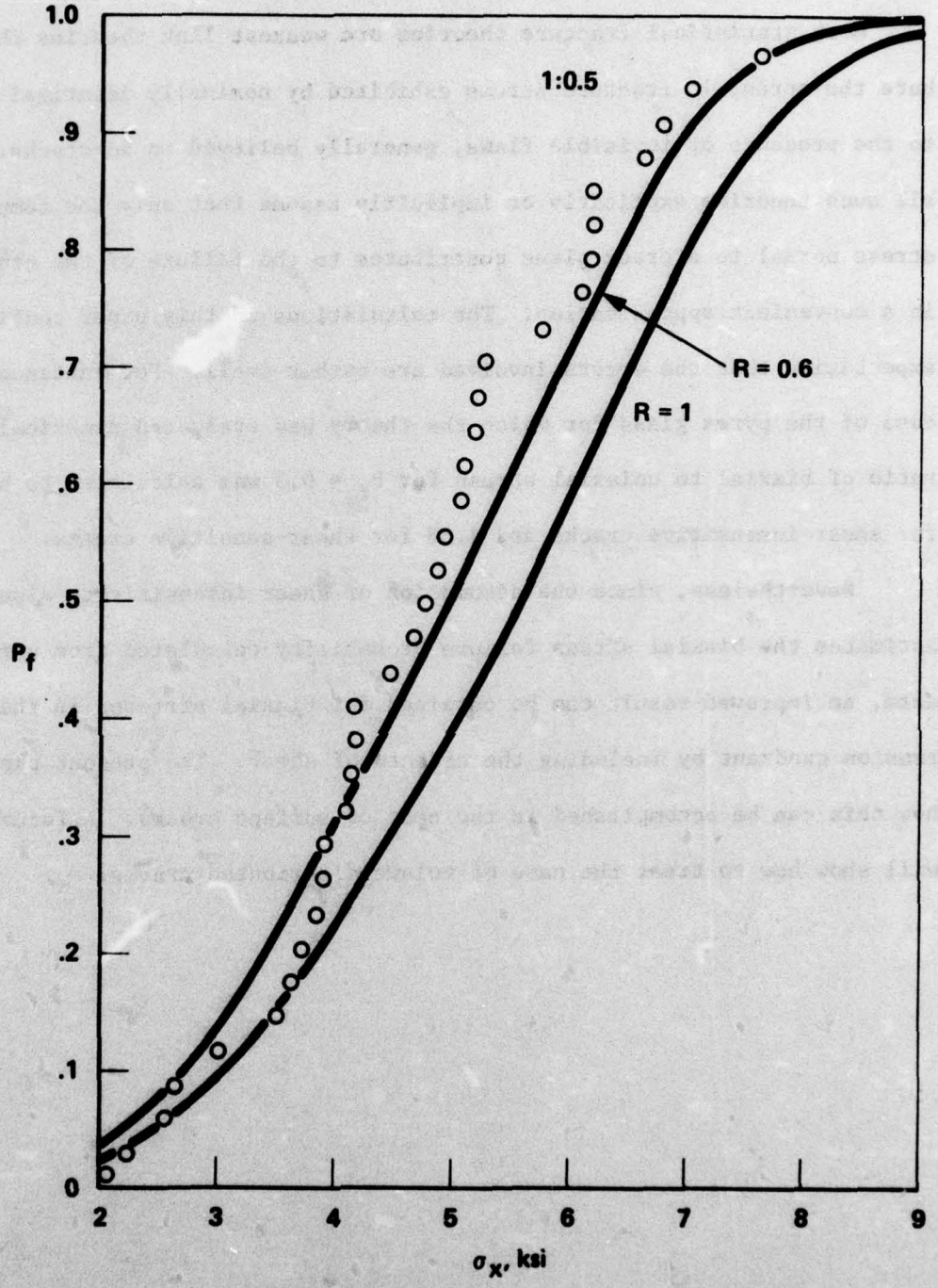

Figure 7. Failure Probability Curves for Stress State 1:0.5 for Isotropically and Anisotropically (R = .6) Distributed Cracks Calculated Using the B(1:1) Fit to the Equibiaxial Data. The points are the 1:0.5 data of Oh (1970).

V. CONCLUDING DISCUSSION

Most statistical fracture theories are weakest link theories that attribute the spread in fracture stress exhibited by nominally identical specimens to the presence of invisible flaws, generally believed to be cracks. Nearly all such theories explicitly or implicitly assume that only the component of stress normal to a crack plane contributes to the failure of the crack. This is a convenient approximation. The calculations in this paper confirm the expectation that the errors involved are rather small. For instance, in the case of the pyrex glass for which the theory was evaluated numerically, the ratio of biaxial to uniaxial stress for $P_f = 0.5$ was calculated to be 1.44 for shear-insensitive cracks and 1.38 for shear-sensitive cracks.

Nevertheless, since the assumption of shear insensitivity always overestimates the biaxial stress failure probability calculated from uniaxial data, an improved result can be obtained for biaxial stresses in the tension-tension quadrant by including the effects of shear. The present paper shows how this can be accomplished in the case of surface cracks. A future paper will show how to treat the case of volume-distributed cracks.

References

Batdorf, S.B. and J.G. Crose (1974), A Statistical Theory for the Fracture of Brittle Structures Subjected to Nonuniform Polyaxial Stresses, J.Appl. Mech. 41, 459.

McClintock, F.A. and A.S. Argon (1966), Mechanical Behavior of Materials, Addison-Wesley, Reading, Mass., 504.

Mirandy, L. and B. Paul (1975), Stresses on the Surface of a Flat Three Dimensional Ellipsoidal Cavity, Trans. ASME 98, 164.

Oh, K.P.L. (1970), On the Statistical Nature of Brittle Fracture, Ph.D. Thesis, University of California, Berkeley.

Oh, K.P.L., O. Vardar and I. Finnie (1973), Failure of Brittle Solids under Biaxial Stresses, Int. J. of Fracture 9, 372.

Paris, P.C., and G.C. Sih (1965), Stress Analysis of Cracks, Fracture Toughness Testing, ASTM STP 381, 30.

Paul, B., and L. Mirandy (1975), An Improved Fracture Criterion for Three Dimensional Stress States, Trans. ASME 98, 159.

Weibull, W. (1939), The Phenomenon of Rupture in Solids, Ingeniors Vetenskaps Akadamien Handlingar, 153.

DISTRIBUTION LIST

Chief of Naval Research
Department of the Navy
Arlington, VA 22217

Attn: Code 474 (2)

Chief of Naval Research
Department of the Navy
Arlington, VA 22217

Attn: Code 471

Chief of Naval Research
Department of the Navy
Arlington, VA 22217

Attn: Code 222

Director
ONR Branch Office
495 Summer Street
Boston, MA 02210

Director
ONR Branch Office
219 S. Dearborn Street
Chicago, IL 60604

Director
Naval Research Laboratory
Attn: Code 2629 (ONRL)
Washington, D.C. 20390 (6)

U. S. Naval Research Laboratory
Attn: Code 2627
Washington, D. C. 20390

Director
ONR - New York Area Office
715 Broadway - 5th Floor
New York, NY 10003

Director
ONR Branch Office
1030 E. Green Street
Pasadena, CA 91101

Defense Documentation Center
Cameron Station
Alexandria, VA 22314 (12)

Commanding Officer
U.S. Army Research Office Durham
Attn: Mr. J. J. Murray
CRD-AA-IP
Box CM, Duke Station
Durham, NC 27706 (2)

Commanding Officer
AMXMR-ATL
Attn: Mr. R. Shea
U.S. Army Materials Res. Agency
Watertown, MA 02172

Watervliet Arsenal
MAGGS Research Center
Watervliet, NY 12189

Attn: Director of Research
Technical Library

Redstone Scientific Info. Center
Chief, Document Section
U.S. Army Missile Command
Redstone Arsenal, AL 35809

Army R&D Center
Fort Belvoir, VA 22060

Commanding Officer and Director
Naval Ship Research & Development Center
Bethesda, MD 20034

Attn: Code 042 (Tech. Lib. Br.)

Commanding Officer and Director
Naval Ship Research & Development Center
Bethesda, MD 20034

Attn: Code 17 (Struc. Mech. Lab.)

Commanding Officer and Director
Naval Ship Research & Development Center
Bethesda, MD 20034

Attn: Code 172

Commanding Officer and Director
Naval Ship Research & Development Center
Bethesda, MD 20034

Attn: Code 172

Commanding Officer and Director
Naval Ship Research & Development Center
Bethesda, MD 20034

Attn: Code 174

Commanding Officer and Director
Naval Ship Research & Development Center
Bethesda, MD 20034

Attn: Code 177

Commanding Officer and Director
Naval Ship Research & Development Center
Bethesda, MD 20034

Attn: Code 1800 (Appl. Math. Lab.)

Commanding Officer and Director
Naval Ship Research & Development Center
Bethesda, MD 20034

Attn: Code 5412S (Dr. W.D. Sette)

Commanding Officer and Director
Naval Ship Research & Development Center
Bethesda, MD 20034

Attn: Code 19 (Dr. M.M. Sevik)

Commanding Officer and Director
Naval Ship Research & Development Center
Bethesda, MD 20034

Attn: Code 1901 (Dr. M. Strassberg)

Commanding Officer and Director
Naval Ship Research & Development Center
Bethesda, MD 20034

Attn: Code 1945

Commanding Officer and Director
Naval Ship Research & Development Center
Bethesda, MD 20034

Attn: Code 196 (Dr. D. Feit)

Commanding Officer and Director
Naval Ship Research & Development Center
Bethesda, MD 20034

Attn: Code 1962

Naval Weapons Laboratory
Dahlgren, VA 22448

Naval Research Laboratory
Washington, D.C. 20375

Attn: Code 8400

Naval Research Laboratory
Washington, D.C. 20375

Attn: Code 8410

Naval Research Laboratory
Washington, D.C. 20375

Attn: Code 8430

Naval Research Laboratory
Washington, D.C. 20375

Attn: Code 8440

Naval Research Laboratory
Washington, D.C. 20375

Attn: Code 6300

Naval Research Laboratory
Washington, D.C. 20375

Attn: Code 6390

Naval Research Laboratory
Washington, D.C. 20375

Attn: Code 6380

Undersea Explosion Research Div.
Naval Ship R&D Center
Norfolk Naval Shipyard
Portsmouth, VA 23709

Attn: Dr. E. Palmer
Code 780

Naval Ship Research & Development Center
Annapolis Division
Annapolis, MD 21402

Attn: Code 2740 - Dr. Y.F. Wang

Naval Ship Research & Development Center
Annapolis Division
Annapolis, MD 21402

Attn: Code 28 - Mr. R.J. Wolfe

Naval Ship Research & Development Center
Annapolis Division
Annapolis, MD 21402

Attn: Code 281 - Mr. R.B. Nierderberger

Naval Ship Research & Development Center
Annapolis Division
Annapolis, MD 21402

Attn: 2814 - Dr. H. Vanderveldt

Technical Library
Naval Underwater Weapons Center
Pasadena Annex
3202 E. Foothill Blvd.
Pasadena, CA 91107

U.S. Naval Weapons Center
China Lake, CA 93557

Attn: Code 4062 - Mr. W. Werback

U.S. Naval Weapons Center
China Lake, CA 93557

Attn: Code 4520 - Mr. Ken Bischel

Commanding Officer
U.S. Naval Civil Engr. Lab.
Code L31
Port Hueneme, CA 93041

Technical Director
U.S. Naval Ordnance Laboratory
White Oak
Silver Spring, MD 20910

Technical Director
Naval Undersea R&D Center
San Diego, CA 92132

Supervisor of Shipbuilding
U.S. Navy
Newport News, VA 23607

Technical Director
Mare Island Naval Shipyard
Vallejo, CA 94592

U.S. Navy Underwater Sound Ref. Lab.
Office of Naval Research
P.O. Box 8337
Orlando, FL 32806

Chief of Naval Operations
Dept. of the Navy
Washington, D.C. 20350

Attn: Code Op07T

Strategic Systems Project Office
Department of the Navy
Washington, D.C. 20390

Attn: NSP-001 Chief Scientist

Deep Submergence Systems
Naval Ship Systems Command
Code 39522
Department of the Navy
Washington, D.C. 20360

Engineering Dept.
U.S. Naval Academy
Annapolis, MD 21402

Naval Air Systems Command
Dept. of the Navy
Washington, D.C. 20360

Attn: NAVAIR 5302 Aero & Structures

Naval Air Systems Command
Dept. of the Navy
Washington, D.C. 20360

Attn: NAVAIR 5308 Structures

Naval Air Systems Command
Dept. of the Navy
Washington, D.C. 20360

Attn: NAVAIR 52031F Materials

Naval Air Systems Command
Dept. of the Navy
Washington, D.C. 20360

Attn: NAVAIR 604 Tech. Library

Naval Air Systems Command
Dept. of the Navy
Washington, D.C. 20360

Attn: NAVAIR 320B Structures

Director, Aero Mechanics
Naval Air Development Center
Johnsville
Warminster, PA 18974

Technical Director
U.S. Naval Undersea R&D Center
San Diego, CA 92132

Engineering Department
U.S. Naval Academy
Annapolis, MD 21402

Naval Facilities Engineering Command
Dept. of the Navy
Washington, D.C. 20360

Attn: NAVFAC 03 Research & Development

Naval Facilities Engineering Command
Dept. of the Navy
Washington, D.C. 20360

Attn: NAVFAC 04 Research & Development

Naval Facilities Engineering Command
Dept. of the Navy
Washington, D.C. 20360

Attn: NAVFAC 14114 Tech. Library

Naval Sea Systems Command
Dept. of the Navy
Washington, D.C. 20360

Attn: NAVSHIP 03 Res. & Technology

Naval Sea Systems Command
Dept. of the Navy
Washington, D.C. 20360

Attn: NAVSHIP 031 Ch. Scientist for R&D

Naval Sea Systems Command
Dept. of the Navy
Washington, D.C. 20360

Attn: NAVSHIP 03412 Hydromechanics

Naval Sea Systems Command
Dept. of the Navy
Washington, D.C. 20360

Attn: NAVSHIP 037 Ship Silencing Div.

Naval Sea Systems Command
Dept. of the Navy
Washington, D.C. 20360

Attn: NAVSHIP 035 Weapons Dynamics

Naval Ship Engineering Center
Prince George's Plaza
Hyattsville, MD 20782

Attn: NAVSEC 6100 Ship Sys Engr & Des Dep

Naval Ship Engineering Center
Prince George's Plaza
Hyattsville, MD 20782

Attn: 6102C Computer-Aided Ship Design

Naval Ship Engineering Center
Prince George's Plaza
Hyattsville, MD 20782

Attn: 6105G

Naval Ship Engineering Center
Prince George's Plaza
Hyattsville, MD 20782

Attn: NAVSEC 6110 Ship Concept Design

Naval Ship Engineering Center
Prince George's Plaza
Hyattsville, MD 20782

Attn: NAVSEC 6120 Hull Div.

Naval Ship Engineering Center
Prince George's Plaza
Hyattsville, MD 20782

Attn: NAVSEC 6120D Hull Div.

Naval Ship Engineering Center
Prince George's Plaza
Hyattsville, MD 20782

Attn: NAVSEC 6128 Surface Ship Struct.

Dean B.A. Boley
Northwestern University
Technological Institute
2145 Sheridan Road
Evanston, IL 60201

Prof. P.G. Hodge, Jr.
University of Minnesota
Dept. of Aerospace Engng. & Mechanics
Minneapolis, MN 55455

Dr. D.C. Drucker
University of Illinois
Dean of Engineering
Urbana, IL 61801

Prof. N.M. Newmark
University of Illinois
Dept. of Civil Engineering
Urbana, IL 61801

Prof. E. Reissner
University of California, San Diego
Dept. of Applied Mechanics
La Jolla, CA 92037

Prof. William A. Nash
University of Massachusetts
Dept. of Mechanics & Aerospace Engng.
Amherst, MA 01002

Library (Code 0384)
U.S. Naval Postgraduate School
Monterey, CA 93940

Prof. Arnold Allentuch
Newark College of Engineering
Dept. of Mechanical Engineering
323 High Street
Newark, NJ 07102

Dr. George Herrmann
Stanford University
Dept. of Applied Mechanics
Stanford, CA 94305

Prof. J. D. Achenbach
Northwestern University
Dept. of Civil Engineering
Evanston, IL 60201

Director, Applied Research Lab.
Pennsylvania State University
P. O. Box 30
State College, PA 16801

Prof. Eugen J. Skudrzyk
Pennsylvania State University
Applied Research Laboratory
Dept. of Physics - P.O. Box 30
State College, PA 16801

Prof. J. Kempner
Polytechnic Institute of Brooklyn
Dept. of Aero. Engrg. & Applied Mech.
333 Jay Street
Brooklyn, NY 11201

Prof. J. Klosner
Polytechnic Institute of Brooklyn
Dept. of Aerospace & Appl. Mech.
333 Jay Street
Brooklyn, NY 11201

Prof. R.A. Schapery
Texas A&M University
Dept. of Civil Engineering
College Station, TX 77840

Prof. W.D. Pilkey
University of Virginia
Dept. of Aerospace Engineering
Charlottesville, VA 22903

Dr. H.G. Schaeffer
University of Maryland
Aerospace Engineering Dept.
College Park, MD 20742

Prof. K.D. Willmert
Clarkson College of Technology
Dept. of Mechanical Engineering
Potsdam, NY 13676

Dr. J.A. Stricklin
Texas A&M University
Aerospace Engineering Dept.
College Station, TX 77843

Dr. L.A. Schmit
University of California, LA
School of Engineering & Applied Science
Los Angeles, CA 90024

Dr. H.A. Kamel
The University of Arizona
Aerospace & Mech. Engineering Dept.
Tucson, AZ 85721

Chief, Airframe & Equipment Branch
FS-120
Office of Flight Standards
Federal Aviation Agency
Washington, D.C. 20553

Chief, Research and Development
Maritime Administration
Washington, D.C. 20235

Deputy Chief, Office of Ship Constr.
Maritime Administration
Washington, D.C. 20235

Attn: Mr. U.L. Russo

Atomic Energy Commission
Div. of Reactor Devel. & Tech.
Germantown, MD 20767

Ship Hull Research Committee
National Research Council
National Academy of Sciences
2101 Constitution Avenue
Washington, D.C. 20418

Attn: Mr. A.R. Lytle

Dr. J. Tinsley Oden
University of Texas at Austin
345 Eng. Science Bldg.
Austin, Texas 78712

Prof. Julius Miklowitz
California Institute of Technology
Div. of Engineering & Applied Sciences
Pasadena, CA 91109

Dr. Harold Liebowitz, Dean
School of Engr. & Applied Science
George Washington University
725-23rd St., N.W.
Washington, D.C. 20006

Prof. Eli Sternberg
California Institute of Technology
Div. of Engr. & Applied Sciences
Pasadena, CA 91109

Prof. Paul M. Naghdi
University of California
Div. of Applied Mechanics
Etcheverry Hall
Berkeley, CA 94720

Professor P. S. Symonds
Brown University
Division of Engineering
Providence, R.I. 02912

Prof. A. J. Durelli
The Catholic University of America
Civil/Mechanical Engineering
Washington, D.C. 20017

Prof. R.B. Testa
Columbia University
Dept. of Civil Engineering
S.W. Mudd Bldg.
New York, N.Y. 10027

Prof. H.H. Bleich
Columbia University
Dept. of Civil Engineering
Amsterdam & 120th St.
New York, N.Y. 10027

Prof. F.L. DiMaggio
Columbia University
Dept. of Civil Engineering
616 Mudd Building
New York, N.Y. 10027

Prof. A.M. Freudenthal
George Washington University
School of Engineering & Applied Science
Washington, D.C. 20006

D.C. Evans
University of Utah
Computer Science Division
Salt Lake City, WA 84112

Prof. Norman Jones
Massachusetts Inst. of Technology
Dept. of Naval Architecture & Marine
Engineering
Cambridge, MA 02139

Professor Albert I. King
Biomechanics Research Center
Wayne State University
Detroit, MI 48202

Dr. V. R. Hodgson
Wayne State University
School of Medicine
Detroit, MI 48202

Naval Ship Engineering Center
Prince George's Plaza
Hyattsville, MD 20782

Attn: NAVSEC 6129 Submarine Struct.

Commander WADD
Wright-Patterson Air Force Base
Dayton, OH 45433

Attn: Code WWRMDD

Commander WADD
Wright-Patterson Air Force Base
Dayton, OH 45433

Attn: Code AFFDL (FDDS)

Commander WADD
Wright-Patterson Air Force Base
Dayton, OH 45433

Attn: Structures Division

Commander WADD
Wright-Patterson Air Force Base
Dayton, OH 45433

Attn: AFLC (MCEEA)

Chief, Applied Mechanics Group
U.S. Air Force Inst. of Tech.
Wright-Patterson Air Force Base
Dayton, Ohio 45433

Chief, Civil Engineering Branch
WLRC, Research Division
Air Force Weapons Laboratory
Kirtland AFB, New Mexico 87117

Air Force Office of Scientific Research
1400 Wilson Blvd.
Arlington, VA 22209

Attn: Mechanics Div.

Structures Research Division
National Aeronautics & Space Admin.
Langley Research Center
Langley Station
Hampton, VA 23365

National Aeronautic & Space Admin.
Associate Administrator for Advanced
Research & Technology
Washington, D.C. 02546

Scientific & Tech. Info. Facility
NASA Representative (S-AK/DL)
P.O. Box 5700
Bethesda, MD 20014

Commandant
Chief, Testing & Development Div.
U.S. Coast Guard
1300 E. Street, N.W.
Washington, D.C. 20226

Technical Director
Marine Corps Dev. & Educ. Command
Quantico, VA 22134

Director
National Bureau of Standards
Washington, D.C. 20234

Attn: Mr. B.L. Wilson, EM 219

Dr. M. Gaus
National Science Foundation
Engineering Division
Washington, D.C. 20550

Science & Tech. Division
Library of Congress
Washington, D.C. 20540

Director
Defense Nuclear Agency
Washington, D.C. 20305

Attn: SPSS

Commander Field Command
Defense Nuclear Agency
Sandia Base
Albuquerque, NM 87115

Director Defense Research & Engrg
Technical Library
Room 3C-128
The Pentagon
Washington, D.C.

DISTRIBUTION LIST

SAMSO
Commander
P.O. Box 92960
Los Angeles, CA 90009

SAMSO
Lt. E. Taylor (RSSE)
P.O. Box 92960
Los Angeles, CA 90009

SAMSO
Capt. C. Logan (RSSE)
P.O. Box 92960
Los Angeles, CA 90009

AFOSR (NA)
Bldg. 410 Bolling Air Force Base
Washington, D.C. 20332

Attn: William J. Walker

USAFA (Library)
USAFA Colorado 80840

AFIT Library (AU)
AFIT, Area B, Bldg. 640
Wright-Patterson AFB, OH 45433

AFML (Library)
Wright-Patterson AFB, OH 45433

AFWL (Library)
Kirtland AFB, NM 87117

AFFDL (Library)
Wright-Patterson AFB, OH 45433

ARL(Library)
Wright-Patterson AFB, OH 45433

Air University Library
(SE) 63-578
Maxwell AFB, AL 36112

University of Pittsburgh
4200 Fifth Ave.
Pittsburgh, PA 15213

Attn: Dr. M. Williams

University of California, Los Angeles
Materials Engineering Department

Attn: Dr. G. Sines

University of California, Los Angeles
Materials Engineering Department

Attn: Dr. W.J. Knapp

University of California, Los Angeles
Materials Engineering Department

Attn: Dr. C.N.J. Wagner

Harvard University
Dept. of Engineering Sciences
Cambridge, MA 02138

Attn: Prof. B. Budiansky

Mitre Corporation
Bedford, MA 02138

Attn: Library

Lockheed Missiles and Space Co.
Sunnyvale, CA 94088
Dept. 81-12, Bldg. 154

Attn: R.D. Teter

Dr. T.H. Lin
Structures and Mechanics Department
School of Engineering and Applied Science
UCLA, Los Angeles, CA 90024

Dr. Lucien Schmit
Structures and Mechanics Department
School of Engineering and Applied Science
UCLA, Los Angeles, CA 90024

Frank J. Seiler Research Laboratories
USAFA, Colorado 80840

Commander
Aeronautical Systems Division
Wright-Patterson AFB, OH 45433

Attn: Library

AFAPL (Library)
Wright-Patterson AFB, OH 45433

AFRPL (Library)
Edwards AFB, California 93523

Naval Weapons Center
China Lake, CA 93555

Attn: W. Herbach, Code 4061

AFFDL (FY) H. Magrath
Wright-Patterson AFB, OH 45433

AFFDL (FB)
Lt. Col. Leigh
Wright-Patterson AFB, OH 45433

AFFDL/FBEDr John Halpin
Wright-Patterson AFB, OH 45433

AFML (MBM) Dr. S.W. Tsai
Wright-Patterson AFB, OH 45433

AFML (MXS)
Capt. C. Budde
Wright-Patterson AFB, OH 45433

Aerospace Corporation
P.O. Box 92957
Los Angeles, CA 90009

Attn: Mr. Norman Au

Aerospace Corporation
P.O. Box 92957
Los Angeles, CA 90009

Attn: Dr. G.W. King

Aerospace Corporation
P.O. Box 92957
Los Angeles, CA 90009

Attn: Library

Commander
Naval Air Development Center
Johnsville, Warminster, PA 18974

Attn: Library

U.S. Naval Academy
Anapolis, MD 21402

Attn: Engineering Department

U.S. Naval Surface Weapons Center
White Oak
Silver Spring, MD 20910

Attn: Library

Commander
U.S. Naval Surface Weapons Center
Dahlgren, VA 22448

Attn: Library

Office of Naval Research
800 North Quincy Street
Arlington, VA 22217

Attn: Mechanics Branch (Code 439)

Director
U.S. Naval Research Laboratory
Washington, D.C. 20390

Attn: Library (Code 2029/ONRL)

Commanding Officer
U.S. Army Advanced Materials
Concept Laboratory
2461 Eisenhower Avenue
Alexandria, VA 23314

Army Research Office
Box CM, Duke Station
Durham, NC 27706

Attn: G. Mayer

Army Research Office
Box CM, Duke Station
Durham, NC 27706

Attn: J. Murray

Army Research Office
Box CM, Duke Station
Durham, NC 27706

Attn: E. Saibel

Commanding Officer
Ballistic Research Laboratory
U.S.A. Aberdeen R&D Center
Aberdeen Proving Ground, MD 21005

Attn: STEAP-TL
(Technical Library Div.)

Commanding Officer
Ballistic Research Laboratory
U.S.A. Aberdeen R&D Center
Aberdeen Proving Ground, MD 21005

Att: Dr. B.E. Cummings

Army Material and Mechanics Research Center
Watertown, MA 02172

Attn: AMXMR-TE (Dr. R. Shea)

Director
Defense Research and Engineering
Room 3E 1063, The Pentagon
Washington, D.C. 20301

NASA
Ames Laboratory
Moffett Field, CA 94045

Attn: Dr. Mel Williams

NASA Langley Research Center
Langley AFB, VA 23365

Attn: Library

NASA Lewis Research Center
21000 Brookpark Road
Cleveland, OH 44135

Attn: Library M. S. 60-3

NASA
George C. Marshall Space Flight Center
Huntsville, AL 35812

Attn: Library

National Science Foundation
1800 G. St. NW
Washington, D.C.

Attn: Dr. C. Astill

National Bureau of Standards
U.S. Department of Commerce
Washington, D.C. 20234

Attn: Technical Reports Section

Dr. Richard C. Bradt
The Pennsylvania State University
University Park, PA 16802

Dr. Jain Finnie
Mechanical Engineering Department
University of California
Berkeley, CA 94720

Mr. J. Fortner
Dept. 248, Bldg 13-3
McDonnel Douglas Aircraft Co.
5301 Bolsa Ave
Huntington Beach, CA 92647

National Science Foundation
1951 Constitution Avenue, NW
Washington, D.C. 20550

Attn: Engineering Sciences Division

Los Alamos Scientific Laboratory
P.O. Box 1665
Los Alamos, NM 87544

Attn: Report Library

Defense Metals Information Center
Battelle Memorial Institute
505 King Avenue
Columbus, OH 43201